Mapping of microelectrostatic fields by means of electron holography: Theoretical and experimental results

J. W. Chen,* G. Matteucci, A. Migliori,† G. F. Missiroli, and E. Nichelatti
Center for Electron Microscopy, Department of Physics, University of Bologna, Via Irnerio 46, 40126 Bologna, Italy

G. Pozzi
Department of Materials Science, University of Lecce, via Arnesano, 73100 Lecce, Italy

M. Vanzi
Quality and Reliability Department, Telettra Società per Azioni, Via Capo di Lucca 31, 40126 Bologna, Italy
(Received 3 October 1988)

The electrostatic field generated by a charged dielectric sphere on a conducting half plane has been investigated both experimentally and theoretically by means of electron holography in a transmission electron microscope. By this technique it is possible to obtain, on the reconstructed image, two-dimensional representations of the in-plane projected potential distribution around the charged sphere. We will show how this example, dealt with in the linear system theory, gives the key to the interpretation of more general plane distributions of potential, for instance, that generated by the reverse-biased *p-n* junctions.

I. INTRODUCTION

Electron holography was first proposed in 1948 by Gabor[1] as a new technique able to increase the resolving power of the electron-microscope images by recording in amplitude and phase the object wave function and then recovering and processing this information by optical means. However, owing to the many experimental difficulties at that time, mainly due to the insufficient level of the instrumentation and the associated technology, electron holography has attained its concrete development in the last decade, thanks to the introduction in electron microscopy of high-brightness electron sources, such as the field emission gun[2] (FEG). With this novel technique, electron phase objects can be investigated. However, until now, only a few applications have been explored (see Refs. 3 and 4 for general reviews), with particular emphasis given so far to the observation of micromagnetic fields, for their fundamental significance (Aharonov-Bohm effect[5]) and practical interest in technological devices.[6,7]

Recently, also the electrostatic field associated with thin reverse-biased *p-n* junctions has been successfully observed.[8] In this case the *p* and *n* regions in the specimen plane give rise to an external field which is not negligible but is, on the contrary, the predominant effect for experiments carried out at standard accelerating voltages (100 kV).[9]

In order to lay the basis for a systematic study by electron holography of microelectrostatic fields (including those generated by a given plane distribution of potential) and to check the sensitivity of the technique we have started by considering the simple field distribution produced by a point charge near a conducting plane.[10] Experimentally, the field is one generated by a specimen made by dielectric microspheres, deposited on a thin carbon conducting film, which become electrically charged under the action of the electron beam.[11] The aim of this paper is to show how electron holography can give a quantitative map of the potential distribution in this elementary case; moreover, how the features of this approach have more general validity as they give the key to solving different but intimately related electrostatic problems, as for instance, the problem referred to above of the field distribution associated with a given plane potential.

The paper is organized in this order: in the following section the basic theoretical and experimental considerations underlying the observation of electric fields by means of electron holography are briefly summarized and the results concerning the mapping of the field distribution generated by charged dielectric spheres on a carbon film are presented. Their theoretical interpretation is treated in Sec. III on the basis of the simple model of a point charge in front of a conducting plane: both the case of infinite and half plane are taken into account. The general problem of the relationship between a given plane distribution of electrostatic potential and the associated phase shift detectable in holographic experiments is then dealt with in Sec. IV and its solution is given within the realm of the linear-system theory. Taking the potential distribution as the input signal and the associated phase shift as the output signal, the kernel of the linear transformation is analytically calculated for the two cases of infinite and half plane. This kernel, corresponding to the phase shift of a pulse potential distribution (Dirac δ function) is shown in Sec. V to be very close, and in the limit of vanishing radius identical, to the experimental phase shift of charged spheres, which therefore can be considered as a nearly ideal probe of the transfer function of the holographic method.

II. ELECTRON HOLOGRAPHY OF ELECTROSTATIC FIELDS

A. General considerations

As is well known, a hologram consists of an interference pattern, normally recorded on a photographic plate, between a wave S scattered by the object under investigation and a reference wave R. The holographic method is able to revive, after suitable processing of the photographic plate, the whole wave S (both in amplitude and in phase) by illuminating the interference pattern with coherent light.

If electrons are used, as shown in Fig. 1, the phase of the wave S is modulated by the object Ob (a thin film perpendicular to the direction of the electron beam) in which electric and or magnetic fields **E** and **B** are present. The reference wave R is taken as that part of the unperturbed electron wave front passing through a hole of the object, possibly in a field-free region. The coherent superposition in the observation plane (OP) of the object and reference waves is provided in the off-axis scheme by the interferometry device (ID), sketched as a prism.

If the object (specimen) contains only weak electric fields so that the potential V can be considered as a small perturbation (at least for experiments carried out at conventional accelerating voltages, i.e., at about 100 kV), the Schrödinger equation can be solved in the high-energy or eikonal approximation[12] and the field can be considered as a pure phase object, characterized by a transmission function given by

$$\psi(x_0,y_0)=e^{i\varphi(x_0,y_0)} , \tag{1}$$

where x_0 and y_0 are the coordinates of a point P in the specimen plane and the phase $\varphi(x_0,y_0)$ is given by

$$\varphi(x_0,y_0)=-\frac{\pi}{\lambda U}\int_{+\infty}^{-\infty} V(x_0,y_0,z)dz , \tag{2}$$

where λ and U are the electron wavelength and the accelerating potential (nonrelativistic approximation), respectively, while the integral is performed along an electron optical ray path antiparallel to the optic axis z (we consider the electron beam propagating from $+\infty$ to $-\infty$; see Fig. 1 for the coordinate system used in this work). The phase φ being proportional to the potential averaged along the electron path, henceforth referred to as projected potential, its knowledge leads to the obtaining of information about the field distribution.

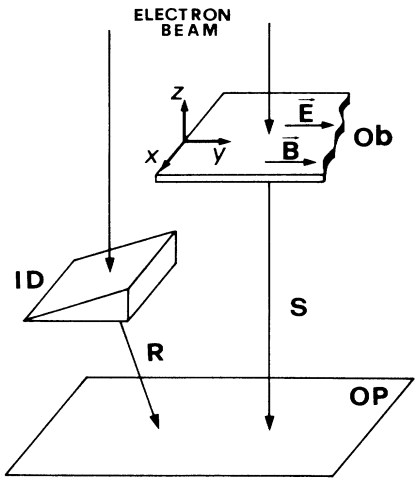

FIG. 1. Basic principle of off-axis hologram formation.

In our particular case the specimen consists of a random distribution of dielectric spheres of radius a deposited on a conducting carbon film. Under the action of the electron beam the latex spheres acquire a stationary positive charge Q as the result of a dynamical equilibrium of charging up by secondary emission, and neutralizing by field emission.[11] The magnitude and the distribution of the stationary charge depend on the material, on the geometry of the scattering object, and on the energy and current density of the electron beam. As regards the field outside the sphere, it can be fairly well approximated by the field of a point charge Q located in the sphere center at a distance a from the conducting grounded plane.[11]

B. Recording and processing of electron holograms

The specimen was prepared by depositing on a carbon film, of about 30 nm in thickness, a little drop of an aqueous suspension of spherical polystyrene latex particles 0.31 μm in diameter. The electron holograms were recorded by the setup schematically shown in Fig. 2. A coherent electron beam, originated by a field emission

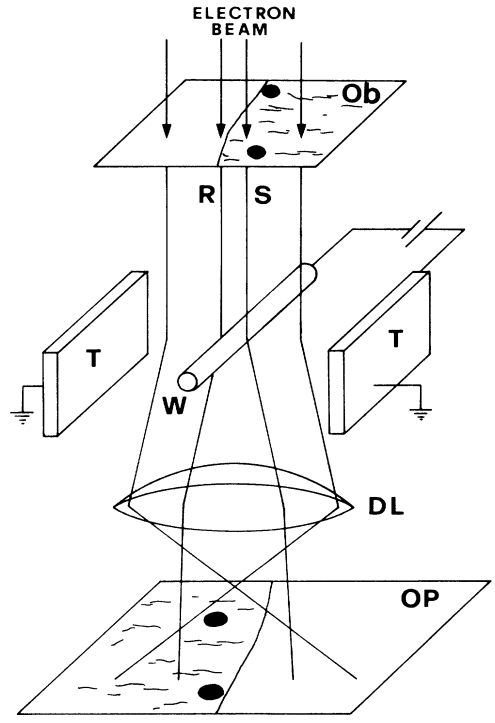

FIG. 2. Schematic experimental setup for off-axis image holography.

source, illuminates the specimen plane in which the object Ob is placed off axis and the reference beam R travels outside the object.

The overall wave front below the specimen plane impinges on the interferometry device,[13] which in our case is a Möllenstedt-Düker electrostatic biprism,[14] inserted at the selected area level. The electron biprism is realized by placing a thin conducting wire W between two earthed plates TT. The wire splits the two waves S and R and, if it is held at a suitable potential, its electrostatic field produces their deflection so that S and R are brought to interfere in the plane OP below the wire.

The microscope, a Philips EM 400 T equipped with a FEG, operated in the diffraction mode with the objective lens switched off; the diffraction lens DL was used to focus the specimen on the photographic plate with a magnification of about 2500×.

The off-axis image holograms recorded in these electron optical conditions have an interference field of about 120 fringes of 85 μm spacing which allow for a resolution referred to the specimen of about 0.1 μm. The retrieval of the information stored in these holograms is performed by processing them in an optical bench with laser light. In this step, after the optical reconstruction of the object wave, a variety of methods can be adopted for recovering and processing the information[4] among which contour mapping and phase amplification will be those used in this work.

The conventional reconstruction of the electron hologram has been carried out in an in-line optical bench equipped with a 10-mW He-Ne laser source. The separation between the reconstructed wave, its twin image and the straight-through beam is accomplished by the filtering aperture placed in the back focal plane of the reconstruction lens. The image is recorded in the screen, whose position along the optical axis can be freely varied and chosen in such a way as to correct the defocus aberration present in the electron hologram.[3,4,6,7] Figure 3(a) shows the focused reconstruction of an electron hologram; only the amplitude information is present in this image, showing a set of six opaque dielectric spheres deposited on the thin carbon film F and the edge of the hole H. Note the presence of two single spheres: A near and B far from the edge of the carbon film F.

Contour maps were performed by two different experimental methods: the first made use of an optical plane-parallel wave which was brought to interfere with the reconstructed object wave;[3,4] the second by recording by the electron microscope, on the same photographic plate, two holograms, one of the object and one with the object withdrawn from the field of view (double exposure holography).[15] In both the cases the final image is crossed by black and white fringes which represent the loci of equal phase, that is, according to Eq. (2), the loci of equal projected potential of the electric field. The phase difference between two neighboring black (or white) fringes is 2π. When an external fringing field is present in the region where the reference wave R propagates (see Fig. 2) double exposure holography allows us to obtain the most reliable contour map as it is free from artifacts introduced in the optical processing, that is the adjustment of the orientation between the reconstructed object wave and the interferometric one.[16] In Fig. 3(b) the contour map of the same region of Fig. 3(a), obtained by the optical reconstruction of the double exposure electron hologram, is shown. Note that the contour-map fringes suffer an abrupt discontinuity when crossing the edge of the film.

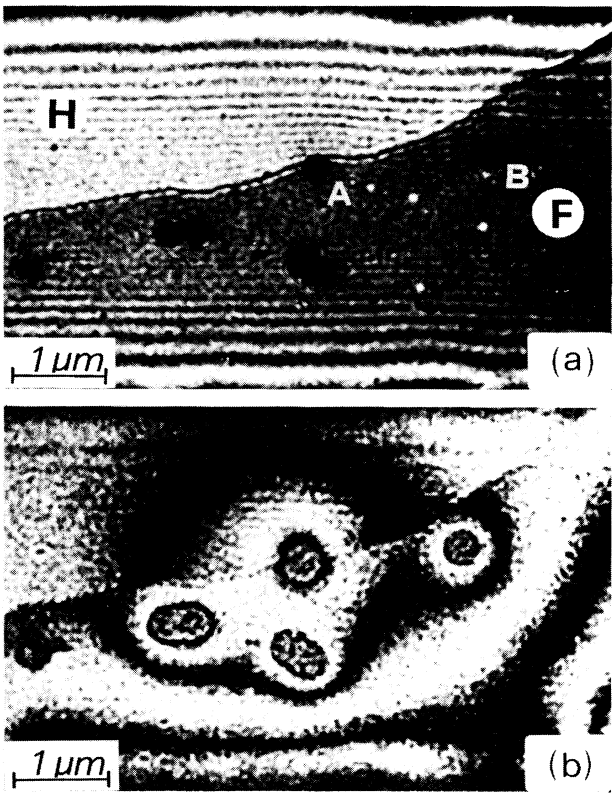

FIG. 3. (a) In-focus optical reconstruction of an electron hologram; (b) optical contour map of the same region.

Phase difference amplification maps, which give more detailed information about the trend of equipotential lines, can be performed either (i) by causing the interference of diffracted conjugated beams after the holographic plate has undergone a suitable nonlinear photographic process[17] (bleaching) or (ii) according to the iterative method suggested by Bryngdahl,[18] both applied in electron holography by Tonomura and co-workers.[4,7] This last method has been used in the present work to obtain the phase amplified contour maps.

Figure 4 shows the optical setup of the Mach-Zehnder interferometer necessary in order to achieve a two-time phase difference amplification. The mirrors are adjusted in such a way as to illuminate the hologram with two beams of different inclinations, so that in the image plane the object wave $(+1)$ and its twin image (-1) are overlapped, thus giving the desired amplification. More generally, $2n$-time amplification can be obtained by overlapping the beams $(+n)$ and $(-n)$. It should be noted that single exposure holograms have been processed since it is impossible to obtain phase difference amplification maps from double exposure electron holograms. Nevertheless,

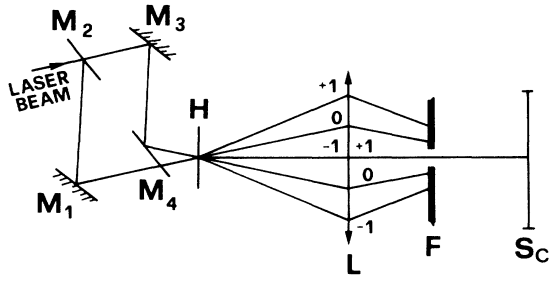

FIG. 4. Optical setup of a Mach-Zehnder interferometer used to perform two-time amplification contour maps. M_1, M_3, reflecting mirrors; M_2, M_4, beam splitters; H, hologram; L, optical reconstructing lens; F, filtering aperture; Sc, final screen.

these latter play an important role as "guide holograms" with which the trend of the contour fringes can be tested. Figure 5(a) shows a two-time amplification contour map of the same region reported in Fig. 3(b) whereas Fig. 5(b) shows a four-time amplification contour map, in which two neighboring equipotential fringes differ in phase of $\pi/2$.

Figures 6(a) and 6(b) show a magnified image of the phase distribution around two single dielectric spheres A and B, respectively, amplified by a factor of 4. It can be seen that whereas the trend of the fringes has a circular symmetry around the particle B which is far from the edge of the carbon film, this symmetry is no longer present for the sphere A located near the edge, i.e., the presence of the edge has a detectable effect on the phase distribution.

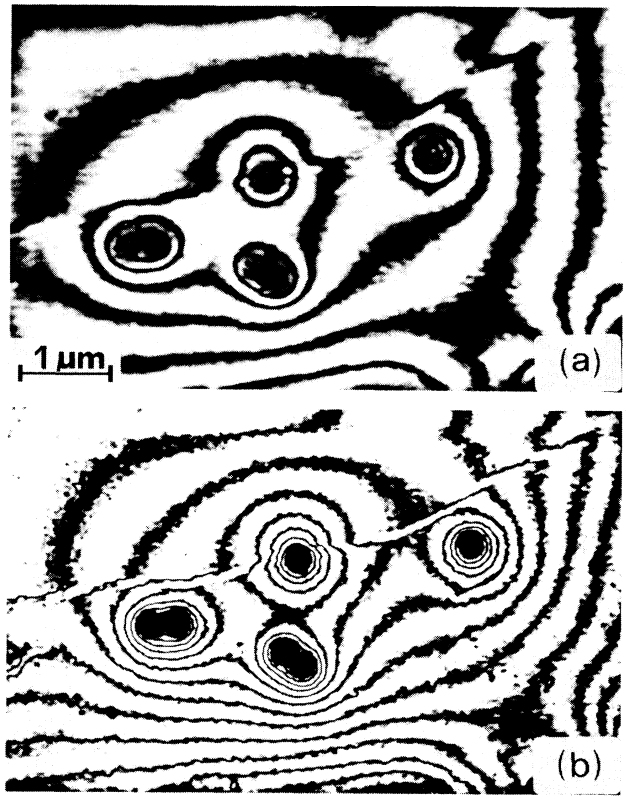

FIG. 5. (a) Two-time and (b) four-time phase difference amplification in contour maps obtained from the same hologram of Fig. 3.

III. INTERPRETATION OF THE EXPERIMENTAL RESULTS

In order to interpret the results of the foregoing paragraph, the electric field around the spherical particles has been modeled by that of a point charge Q localized in the sphere center and placed in front of a conducting plane. For a particle far from the edge, whose center is positioned at the point (x_0,y_0,a), the potential in the half space $z>0$ can be calculated by means of the image charge method,[10] and is given by the expression

$$V(x,y,z)=\frac{Q}{4\pi\epsilon_0}\left[\frac{1}{[(x-x_0)^2+(y-y_0)^2+(z-a)^2]^{1/2}}-\frac{1}{[(x-x_0^2)+(y-y_0)^2+(z+a)^2]^{1/2}}\right] \tag{3}$$

[while in the half space $z<0$ $V(x,y,z)=0$] from which the phase shift φ according to Eq. (2) can be calculated analytically. It follows that

$$\varphi(x,y)=\frac{Q}{2\epsilon_0\lambda U}\operatorname{arcsinh}\left[\frac{a}{[(x-x_0)^2+(y-y_0)^2]^{1/2}}\right], \tag{4}$$

where ϵ_0 is the dielectric constant of vacuum.

Simulations of the contour map images produced by the phase distribution (4), in which the edge effects of the carbon film have been momentarily neglected, have been carried out using an IBM PC/AT equipped with a video board able to display 512×512 pixels at 256 grey levels.

Figure 7 shows the results for our point-charge distribution of Fig. 3(a) assuming $Q=400e=6.4\times10^{-17}$ G and $a=0.155$ μm. This value of the charge is in agreement with the findings of Komrska,[11] who measured a charge of $1100e$ on spheres of radius 0.28 μm by studying their electron diffraction patterns.

The overall similarity between calculated and experimental images is satisfying far from the edge, thus confirming the main hypotheses made and allowing, within this framework, the determination of the charge Q with an accuracy of 20%. Of course, near the edge, differences are detectable due to the fact that the simple model does not take into ac-

count the discontinuity of the conducting film.

If the actual shape of the edge is replaced by a straight line, the electrostatic problem still has an analytical solution.[19] Referring to Fig. 8 for the definition of α and ϑ, the solution reads

$$V(x,y,z)=\frac{Q}{2\pi^2\epsilon_0}(h_- - h_+) , \tag{5}$$

where

$$h_\pm=\frac{1}{[r^2+(z\pm a)^2]^{1/2}}\arctan\left[\frac{[(\rho+r_0)^2+(x-x_0)^2]^{1/2}+\gamma_\pm[2(\rho r_0+yy_0\mp za)]^{1/2}}{[r^2+(z\pm a)^2]^{1/2}}\right] \tag{6}$$

and

$$\begin{aligned} r_0&=(a^2+y_0^2)^{1/2} ,\\ r&=[(x-x_0)^2+(y-y_0)^2]^{1/2} ,\\ \rho&=(y^2+z^2)^{1/2} , \end{aligned} \tag{7}$$

$$\gamma_+=\begin{cases} 1, & \vartheta\in[0,\pi-\alpha[\\ -1, & \vartheta\in[\pi-\alpha,2\pi[\end{cases} , \tag{8}$$

$$\gamma_-=\begin{cases} 1, & \vartheta\in[0,\pi+\alpha[\\ -1, & \vartheta\in[\pi+\alpha,2\pi[\end{cases} . \tag{9}$$

Since no analytical expression for the phase shift was found, it has been calculated by numerical integration of Eq. (2) with the potential distribution (5).

Figure 9 shows the results of the contour-map simulation for the charged sphere on the whole or on the half plane. Here again it can be ascertained that the effect of the edge is to break the circular symmetry of the contour lines around the particle and that their distortion increases as the particle approaches the edge. However, it is not responsible for the step observed experimentally, which is entirely due to, and can be properly accounted for, by the introduction of a constant phase shift in the half plane due to the mean inner potential of the carbon film.

IV. IMPULSE RESPONSE FUNCTION FOR A GIVEN PLANE POTENTIAL DISTRIBUTION

A. General considerations

In order to recognize the deep physical implications of the above experiments and calculations, let us turn now to the case of the three-dimensional electrostatic field generated by a given plane potential distribution. The basic idea is that of characterizing the connection between the potential distribution on the plane (assumed to be perpendicular to the direction of the electron beam,

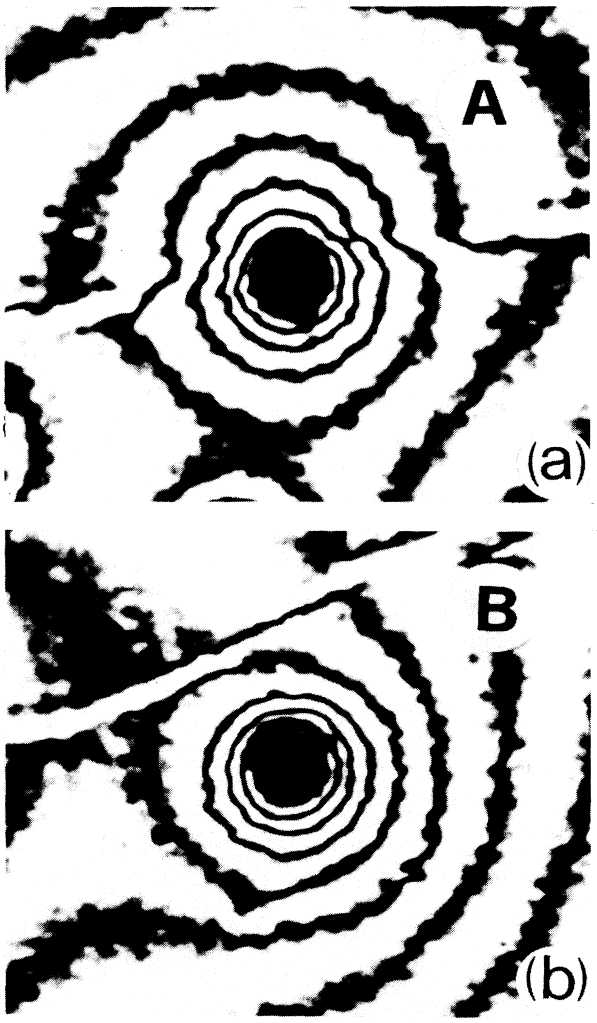

FIG. 6. Four-time phase difference amplification in contour map of the single charged spheres labeled *A* and *B* in Fig. 3.

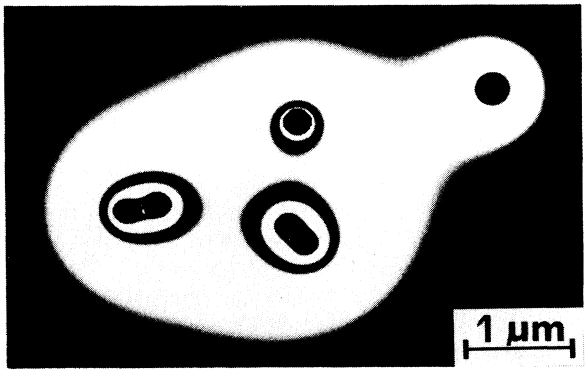

FIG. 7. Simulated contour map for the same distribution of charged spheres as shown in Fig. 3.

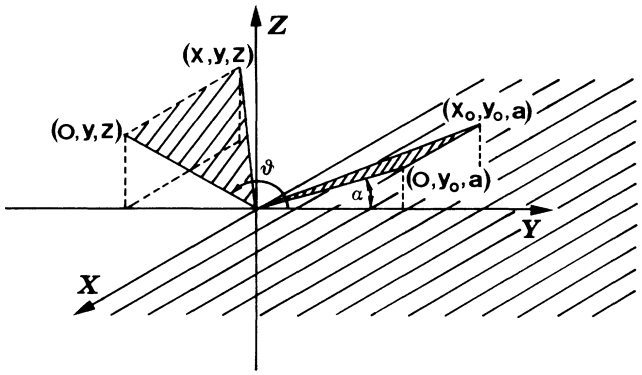

FIG. 8. Coordinate system for the potential and phase calculation in the conducting half-plane problem. (x_0,y_0,a), position of the point charge; (x,y,z) observation point; $(0,y_0,a)$, projection of the position of the point charge on plane $0yz$; $(0,y,z)$, projection of the observation point on plane $0yz$.

axis z) and the electron-beam phase shift by means of an impulse response function, as suggested by the linear-system theory.

Let us recall that the external field associated with a thin plane specimen containing reverse-biased p-n junctions is a very interesting example of such a case. In the actual experiment, the potential distribution in the whole space is of course univocally defined by the transmission electron microscope (TEM) column geometry together with the values of the potential on the upper and lower surfaces of the specimen, and therefore in general its three-dimensional form is not easy to describe, so Eq. (2) is of very little practical aid.

The problem becomes more manageable if the assumption is made that the TEM column walls are so far from the beam and the specimen region that this latter can be considered as the only structure present in the space. Moreover, the same bidimensional potential distribution $V_0(x_0,y_0)$ is assumed to exist both inside and on the upper and lower specimen surfaces. Finally, the effect of the specimen thickness on the field is neglected.

With these assumptions, a classical theorem in electrostatics, known as the Green reciprocity theorem, states that the potential distribution $V(x,y,z)$ in the empty space outside the plane is given by

$$V(x,y,z)=-\frac{1}{q}\int\int_{\Sigma}\sigma_{\Sigma}(x_0,y_0;x,y,z)V_0(x_0,y_0)\times dx_0dy_0 \ , \tag{10}$$

where $V_0(x_0,y_0)$ is the known voltage distribution on the plane surface Σ, whose area infinitesimal element is dx_0dy_0 and $\sigma_{\Sigma}(x_0,y_0;x,y,z)$ is the charge density which would be induced at the point (x_0,y_0) of Σ, if it were a grounded conducting surface, by a unit charge $q=1$ C located in (x,y,z).

This gives the following expression for the phase shift $\varphi(x,y)$ due to the external field:

$$\varphi(x,y)=\int\int_{\Sigma}V_0(x_0,y_0)f_{\Sigma}(x,y;x_0,y_0)dx_0dy_0 \ , \tag{11}$$

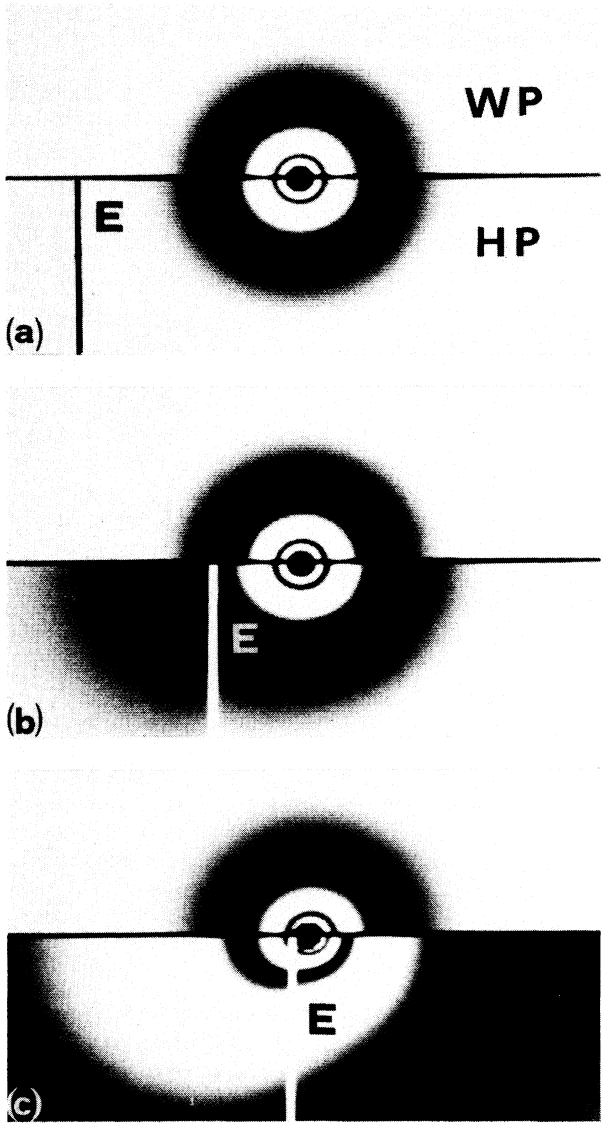

FIG. 9. Comparison of simulated contour maps of a single charged sphere located on the whole conducting plane WP (upper part of each picture) and near the edge (lower part) of a half conducting plane HF. The vertical white line E marks the edge position. Distance between the sphere and the edge: (a) 5 μm; (b) 2 μm; (c) 0.155 μm.

with

$$f_{\Sigma}(x,y;x_0,y_0)=\frac{\pi}{q\lambda U}\int_{+\infty}^{-\infty}\sigma_{\Sigma}(x_0,y_0;x,y,z)dz$$
$$=\frac{\pi}{q\lambda U}\int_{+\infty}^{-\infty}[\sigma_{+}(x_0,y_0;x,y,z)+\sigma_{-}(x_0,y_0;x,y,z)]dz \ , \tag{12}$$

where σ_{+} and σ_{-} are the surface charge densities which would appear on the upper and lower side of the surface Σ, respectively, if it were a grounded conductor faced to

a point charge in (x,y,z). The value of the charge density is, of course, zero outside Σ, i.e., the physical extension of the specimen (e.g., into its holes).

The above situation corresponds to a specimen of negligible thickness, supporting the given potential distribution; the correction to the phase due to the finiteness of the thickness t of an actual specimen can be taken into account by adding the phase shift

$$\Delta\varphi(x,y)=-\frac{\pi t}{\lambda U}[V_m+V_0(x,y)] , \tag{13}$$

where, we recall, it has been assumed that the same bidimensional distribution $V_0(x_0,y_0)$ is present on both the faces of the specimen and inside, and V_m is the mean inner potential. As this correction is small and can be neglected in a first approximation, we refer henceforth to the external field only.

The relevance of Eq. (11) is due to its resemblance to the general equation describing a bidimensional linear transmission system, having V_0 as the input, φ as the output, and f_Σ as the impulse response function,[20] independent of the actual input or output, and summarizing all the features and performances of the system. Its careful evaluation should give the key to model the system, simulating its response.

There are two ways to obtain the impulse response function of a linear system: either calculating or measuring it. The first approach often requires skillful theoretical work, while the second needs the availability of a "pulse" input function, as similar as possible to an ideal pulse. Such a pulse, mathematically described by a Dirac δ distribution, inserted in Eq. (11), produces a response φ_δ equal to the transmission function f_Σ:

$$\varphi_\delta(x,y)=f_\Sigma(x,y;x_0,y_0) . \tag{14}$$

However, it should be stressed once more that each evaluation of f_Σ holds for any voltage distribution on the surface of specimens of the same shape, the physical meaning of f_Σ being that of the mean surface charge density induced on a grounded film of the same shape as the specimen by means of a point charge traveling along a straight line parallel to z. Therefore the theoretical approach has been limited to the two most significant cases: the whole-plane and the half-plane problems. The mathematical effort for the solution of the latter will give an idea of the difficulties of this approach in the general case.

B. The whole-plane problem

A unit point charge $q=1$ C located at (x,y,z) above a grounded conducting plane, whose equation is $z=0$, gives rise to a potential distribution which can be simply evaluated by means of the image charge method. The use of the laws of electrostatics allows the calculation of the expressions for the charge densities σ_+ and σ_- which appear at the point (x_0,y_0) on the upper and lower face of the conducting plane, respectively, once the potential distribution, Eq. (3), is known. Simple calculations give

$$\sigma_+(x_0,y_0;x,y,z)=\begin{cases}-\dfrac{q}{2\pi}\dfrac{z}{(r^2+z^2)^{3/2}}, & z\geq 0\\ 0, & z<0\end{cases} \tag{15}$$

$$\sigma_-(x_0,y_0;x,y,z)=\begin{cases}0, & z\geq 0\\ \dfrac{q}{2\pi}\dfrac{z}{(r^2+z^2)^{3/2}}, & z<0\end{cases} \tag{16}$$

where, as stated in Eq. (7), r is given by

$$r=[(x-x_0)^2+(y-y_0)^2]^{1/2} \tag{17}$$

so that

$$\sigma_++\sigma_-=-\frac{q}{2\pi}\frac{|z|}{(r^2+z^2)^{3/2}} , \tag{18}$$

which gives, by integration of Eq. (12), the impulse response function, already reported in Ref. 21:

$$f_{\mathrm{WP}}(x,y;x_0,y_0)=\frac{1}{\lambda U r} , \tag{19}$$

where WP means "whole plane."

C. The half-plane problem

In complete analogy with the above case, we start from Eq. (5) giving the expression for the potential distribution associated with the unit point charge $q=1$ C at (x,y,z) and the grounded half plane $z=0$, $y\geq 0$.

The charge densities on the upper and lower face of the half plane can now be calculated and it follows that

$$\sigma_\pm(x_0,y_0;x,y,z)=\mp\frac{qz}{4\pi R^3}-\frac{q}{4\pi}\left\{\frac{2}{\pi R^2}\left[\frac{(y^2+z^2)^{1/2}-y}{2y_0}\right]^{1/2}+\frac{2}{\pi}\frac{z}{R^3}\arctan\left[\frac{z}{R}\left[\frac{2y_0}{(y^2+z^2)^{1/2}-y}\right]^{1/2}\right]\right\} , \tag{20}$$

where

$$R=(r^2+z^2)^{1/2} . \tag{21}$$

It follows that

$$\sigma_++\sigma_-=-\frac{q}{\pi^2}\frac{z}{R^3}\left\{\frac{R}{z}\left[\frac{(y^2+z^2)^{1/2}-y}{2y_0}\right]^{1/2}+\arctan\left[\frac{z}{R}\left[\frac{2y_0}{(y^2+z^2)^{1/2}-y}\right]^{1/2}\right]\right\} . \tag{22}$$

An integration by parts, followed by the relevant substitution

$$\eta=\left[\frac{r}{y+(y^2+z^2)^{1/2}}\right]^{1/2}, \tag{23}$$

enables the calculation of f_{HP} (HP means "half plane"), according to integral (12):

$$f_{\mathrm{HP}}(x_0,y_0;x,y)=\begin{cases}\dfrac{1}{\lambda U r}\left[\dfrac{r-y+y_0}{y_0}\right]^{1/2}, & y\le 0\\ \dfrac{1}{2\lambda U r}\left[\dfrac{r-y+y_0}{y_0}\right]^{1/2}+\dfrac{2}{\pi\lambda U r}\arctan\left[\dfrac{\sqrt{yy_0}}{r}\right]\\ +\dfrac{1}{\pi\lambda U r}\left[\dfrac{r-y+y_0}{y_0}\right]^{1/2}\arctan\left[\dfrac{r-2y}{2[y(r-y+y_0)]^{1/2}}\right]\\ +\dfrac{1}{\pi\lambda U r}\left[\dfrac{r+y-y_0}{y_0}\right]^{1/2}\operatorname{arctanh}\left[\dfrac{2[y(r+y-y_0)]^{1/2}}{r+2y}\right], & y>0\ .\end{cases} \tag{24}$$

For large values of both y and y_0 in the half plane, the impulse response function f_{HP} recovers the behavior of the function f_{WP} found for the whole plane, as one can directly verify.

V. CHARGED SPHERES AND IMPULSE RESPONSE FUNCTION

The two parallel items which have been dealt with up to now, namely, the phase shift associated with charged particles on a conducting film and the impulse response function relating a phase shift to the given plane potential distribution, will emerge and show a deep connection as the size of the spheres becomes smaller.

Both for the whole and the half plane, indeed, the potential distribution induced at the generical point (x,y,z) by a point charge Q (representing the charged sphere) located at (x_0,y_0,a) is expressed as a difference between two values of a function g calculated in two different points [see Eqs. (3) and (5)]:

$$V(x,y,z)=g(x,y,z;x_0,y_0,a)-g(x,y,z;x_0,y_0,-a)\ . \tag{25}$$

Since the following relation holds (both for the whole- and the half-plane case):

$$\lim_{a\to 0}[g(x,y,z;x_0,y_0,a)-g(x,y,z;x_0,y_0,-a)]=\lim_{a\to 0}[g(x,y,z+a;x_0,y_0,0)-g(x,y,z-a;x_0,y_0,0)]\ , \tag{26}$$

we find that, as the radius a of the sphere decreases, the difference (25) approaches an actual differential ratio:

$$V(x,y,z)=2a\frac{\partial g}{\partial z}(x,y,z;x_0,y_0,0)+o(a)\quad(a\to 0)\ , \tag{27}$$

where $o(a)/a$ approaches zero as a becomes vanishingly small.

On the other hand, the total charge density $\sigma_+ +\sigma_-$ induced on the conducting surface by an exploring charge $q=1$ C located in (x_0,y_0,a) is proportional to the electric field $\mathbf{E}_n$ normal to that surface:

$$\begin{aligned}\sigma_+(x,y)+\sigma_-(x,y)&=-\frac{q}{Q}\lim_{z\to 0}\epsilon_0\frac{\partial V}{\partial z}(x,y,z)\\ &=-\frac{q}{Q}\epsilon_0\lim_{z\to 0}\left[\frac{\partial g}{\partial z}(x,y,z;x_0,y_0,a)-\frac{\partial g}{\partial z}(x,y,z;x_0,y_0,-a)\right]\end{aligned} \tag{28}$$

and it is easy to see that

$$\sigma_+(x,y)+\sigma_-(x,y)=-2\epsilon_0\frac{q}{Q}\frac{\partial g}{\partial z}(x,y,0;x_0,y_0,a)\ . \tag{29}$$

The important consequence of the above results is that, when the charged sphere is so small as to be considered part of the conducting surface, the voltage distribution $V_0(x,y)$ of the surface itself is given by

$$\lim_{a\to 0}V_0(x,y)=\lim_{a\to 0}V(x,y,0)=\lim_{a\to 0}\left[2a\frac{\partial g}{\partial z}(x,y,0;x_0,y_0,0)\right]=-\frac{Q}{q}\lim_{a\to 0}\frac{a}{\epsilon_0}(\sigma_+ +\sigma_-)\ , \tag{30}$$

$$V_0(x,y)=-\frac{Q}{q}\frac{a}{\epsilon_0}\lim_{a\to 0}(\sigma_+ +\sigma_-)+o(a)\quad(a\to 0)\ . \tag{31}$$

Referring to the expression of $\sigma_+ + \sigma_-$ [Eqs. (18) and (22)] we find

$$\lim_{a\to 0}\left[\frac{\sigma_+ + \sigma_-}{q}\right] = \begin{cases} 0 & \text{if } (x,y)\neq(x_0,y_0) \\ -\infty & \text{if } (x,y)=(x_0,y_0) \end{cases} \tag{32}$$

and also, after lengthy calculations for the half-plane solution:

$$\frac{1}{q}\int\int_{\Sigma}[\sigma_+(x,y)+\sigma_-(x,y)]dx\,dy = -1 \quad \forall a\ , \tag{33}$$

where Σ indicates the whole or the half plane accordingly. The last two expressions only state that $(\sigma_+ + \sigma_-)/q$ becomes a negative Dirac δ function when a vanishes; therefore for the small charged sphere, we have

$$V_0(x,y) = \frac{a}{\epsilon_0} Q\delta(x-x_0,y-y_0) + o(a) \quad (a\to 0)\ . \tag{34}$$

The phase shift associated with such an infinitesimal charged sphere on the conducting planar surface Σ is consequently

$$\varphi(x,y) = \frac{aQ}{2\epsilon_0} f_{\Sigma}(x,y;x_0,y_0) \tag{35}$$

(the factor $\frac{1}{2}$ appears since the δ function is present only in one of the two faces of the specimen, the other being completely grounded). Apart from a constant factor, the foregoing formula is the impulse response function of the bidimensional linear transmission system with Σ as the specimen surface, where a planar voltage distribution is given.

In practice, of course, the size of the particles is not negligible, and this should be taken into account. For the whole plane it is possible to have an analytical expression for the phase shift due to both a finite-size particle of charge Q:

$$\varphi(x,y) = \frac{Q}{2\epsilon_0 \lambda U}\operatorname{arcsinh}\left[\frac{a}{r}\right] \tag{36}$$

and an ideal pulse of the same amplitude

$$\varphi(x,y) = \frac{Qa}{2\epsilon_0}\frac{1}{\lambda U r} = \frac{Qa}{2\epsilon_0} f_{\Sigma}(x,y;x_0,y_0) \tag{37}$$

and a comparison of the two results shows that the difference falls below 1% at $r > 2.5a$, which can be accepted as the limit for the validity of the approximation.

Figure 10 compares the expected contour maps for a sphere of radius $a = 0.155$ μm with a point charge of the same value. The quick convergence of the two patterns is clear when the distance from the centers increases.

For the half plane, an analytical expression of the phase shift associated with the finite-size particle was not

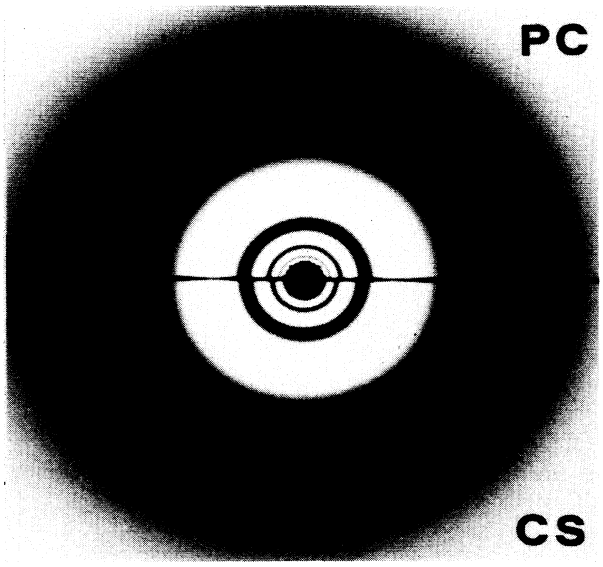

FIG. 10. Comparison between simulated contour maps of a point charge PC (upper part of the picture) and a sphere CS (lower part) of 0.31 μm in diameter having the same charge for the whole-plane case.

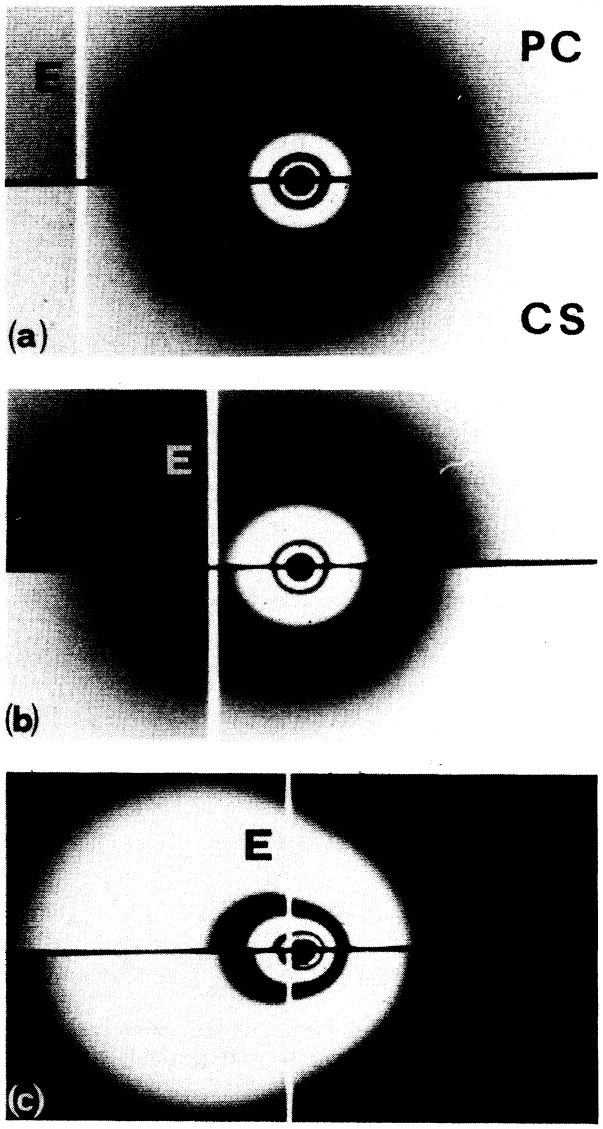

FIG. 11. Comparison between simulated contour maps of a point charge PC and a charged sphere CS. Distance of the charge center from the edge E for the half plane: (a) 5 μm; (b) 2 μm; (c) 0.155 μm.

found, making it impossible to give a direct evaluation of the approximation.

A simulation analogous to Fig. 10 was performed with the same conditions and for different distances of the particles from the edge, by numerically integrating the expression for the potential, as reported in Fig. 11. Here not only the absolute distance of the particle from the edge is important, but also the ratio between the particle size and its distance from the edge. When this ratio is small, the solution of the whole plane is valid near the particle. On the other hand, when this ratio increases, a strong distortion of the phase pattern takes place. In any case, the trend of the equiphase lines is well comparable with the pattern produced by the point charge.

VI. CONCLUSIONS

In this work we have tried to explain the deep connections between two apparently different problems which are encountered in the investigation of electrostatic fields by means of the electron holography technique in a transmission electron microscope, namely, that of charged dielectric spheres on a conducting film and that of plane potential distributions (for example, those generated in a thin reverse-biased *p-n* junction), both electron optical phase objects. Apart from the many practical implications, some not trivial physical considerations result from our investigation: the main conclusion is that in this case the holographic electron microscope can be considered as a two-dimensional linear transmission system, encoding a bidimensional plane voltage input information in an output phase distribution, measurable by means of contour-mapping methods. The function characterizing all the features of the system (impulse response) has been calculated theoretically for the two cases of the whole and the half plane, and has been shown to be very similar to the phase shift caused by small charged dielectric spheres. This conclusion is likely to hold for any planar shape of the specimen. Therefore the impulse response function for an arbitrary plane distribution of electrostatic voltage, even if it cannot be calculated by analytical methods, can be experimentally investigated by the observation of the phase shift caused by a small charged sphere deposited on the specimen surface, held at ground potential. The knowledge of the impulse response function for any given specimen shape can answer some important questions concerning electron holography of electrostatic fields such as "How much does the shape of the edge affect the phase distribution inside the specimen? or "How far from the specimen edge is a region of negligible field available, through which the holographic reference wave can travel without being perturbed by the leakage fields?" These questions will be the subject of future investigations.

Finally it should be remarked that the unsuspected relation between the two problems can be justified by the *a posteriori* recognition that the field of the point charge near a conducting plane plays the same basic role in the electron holography of given plane distribution of potential as the field of a point charge in electrostatics.

ACKNOWLEDGMENTS

The skillful technical assistance of S. Patuelli is gratefully acknowledged. This work has been supported by funds from Ministero della Pubblica Istruzione, Italia, Dr. J. W. Chen carried out this work with the support of the International Centre for Theoretical Physics Program for Training and Research in Italian Laboratories, Trieste, Italy. J. W. C., G. M., A. M., G. F. M., E. N., and G. P. are all affiliated with the Consozzio Interuniversitario di Struttura della Materia and the Consiglio Nazionale delle Ricerche-Gruppo Nazionale di Struttura della Materia.

---

*On leave from Shanghai Institute of Optics and Fine Mechanics, Academia Sinica, P.O. Box 8216, Shanghai, China.

†Present address: Laboratorio dei Materiali per l'Elettronica, Consiglio Nazionale delle Ricerche, via de Castagnoli 1, 40126 Bologna, Italy.

[1]D. Gabor, Nature (London) **161**, 777 (1948); Proc. R. Soc. London Ser. A **197**, 454 (1949); Proc. R. Soc. London Ser. B **64**, 449 (1951).

[2]J. F. Hainfeld, in *Scanning Electron Microscopy 1977*, edited by O. Jahari (IITRI Chicago, 1977), Vol. 1, p. 591.

[3]K. J. Hanszen, Adv. Electron. Electron Phys. **59**, 1 (1982); J. Phys. D **19**, 373 (1986).

[4]A. Tonomura, Prog. Opt. **23**, 185 (1986); Rev. Mod. Phys. **59**, 639 (1987).

[5]Y. Aharonov and D. Bohm, Phys. Rev. **115**, 485 (1959).

[6]G. Matteucci, G. F. Missiroli, and G. Pozzi, IEEE Trans. Magn. **20**, 1970 (1984).

[7]A. Tonomura, J. Appl. Phys. **61**, 4297 (1987).

[8]S. Frabboni, G. Matteucci, G. Pozzi, and M. Vanzi, Phys. Rev. Lett. **55**, 2196 (1985); S. Frabboni, G. Matteucci, and G. Pozzi, Ultramicroscopy **23**, 29 (1987).

[9]P. G. Merli and G. Pozzi, Optik (Stuggart) **51**, 39 (1978); G. Pozzi, *ibid.* **53**, 381 (1979).

[10]R. P. Feynman, *The Feynman Lectures in Physics* (Addison-Wesley, Reading, MA, 1967), Vol. 2.

[11]V. Drahoš, J. Komrska, and M. Lenc, Z. Angew. Phys. **27**, 227 (1969); J. Komrska, in *Advances in Electronics and Electron Physics* (Academic, New York, 1971), Vol. 30, p. 139.

[12]L. D. Landau and E. M. Lifshitz, *Quantum Mechanics* (Pergamon, Oxford, 1965); K. Gottfried, *Quantum Mechanics* (Benjamin, London, 1966).

[13]G. F. Missiroli, G. Pozzi, and U. Valdrè, J. Phys. E **14**, 649 (1981).

[14]G. Möllenstedt and H. Düker, Naturwissenschaften **42**, 41 (1955); Z. Phys. **145**, 377 (1956).

[15]H. Wahl, Ph.D. thesis, University of Tübingen, 1975.

[16]G. Matteucci, G. F. Missiroli, J. W. Chen, and G. Pozzi, Appl. Phys. Lett. **52**, 176 (1988).

[17]K. Matsumoto and M. Takahashi, J. Opt. Soc. Am. **60**, 30 (1970).
[18]O. Bryngdahl, J. Opt. Soc. Am. **59**, 142 (1969).
[19]E. Durand, *Electrostatique* (Masson, Paris, 1966), Vol. 2, p. 231.
[20]J. W. Goodman, *Introduction to Fourier Optics* (McGraw-Hill, New York, 1968).
[21]M. Vanzi, Optik (Stuttgart) **68**, 319 (1984).

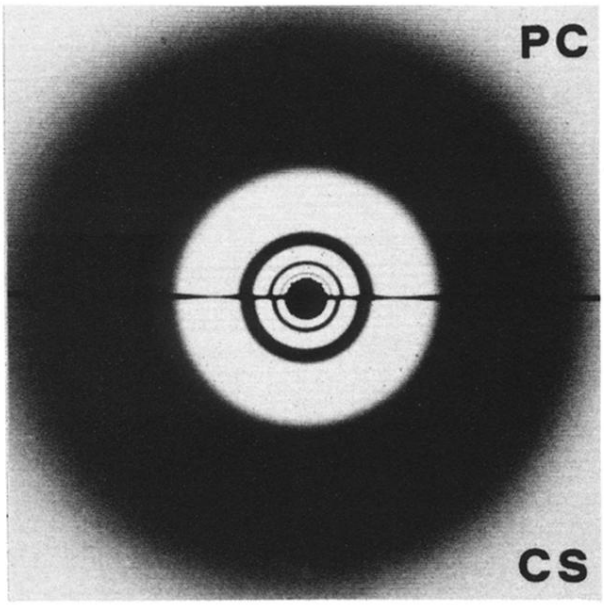

FIG. 10. Comparison between simulated contour maps of a point charge PC (upper part of the picture) and a sphere CS (lower part) of 0.31 μm in diameter having the same charge for the whole-plane case.

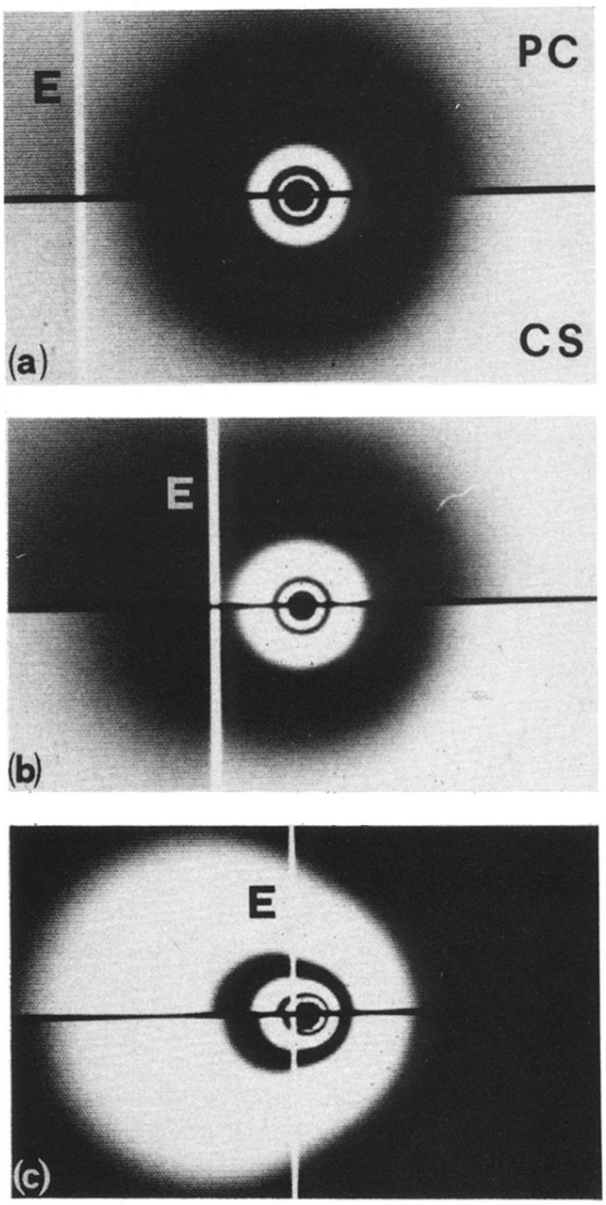

FIG. 11. Comparison between simulated contour maps of a point charge PC and a charged sphere CS. Distance of the charge center from the edge E for the half plane: (a) 5 μm; (b) 2 μm; (c) 0.155 μm.

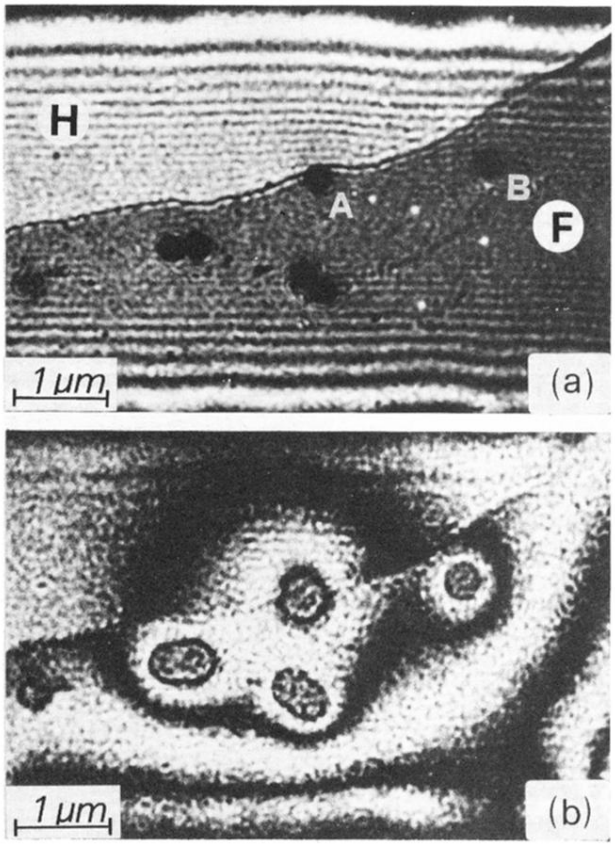

FIG. 3. (a) In-focus optical reconstruction of an electron hologram; (b) optical contour map of the same region.

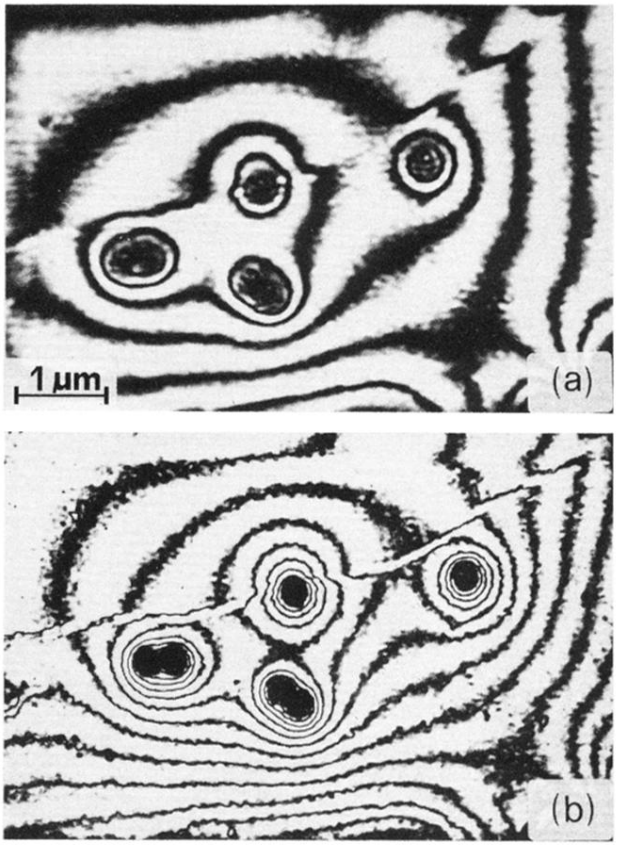

FIG. 5. (a) Two-time and (b) four-time phase difference amplification in contour maps obtained from the same hologram of Fig. 3.

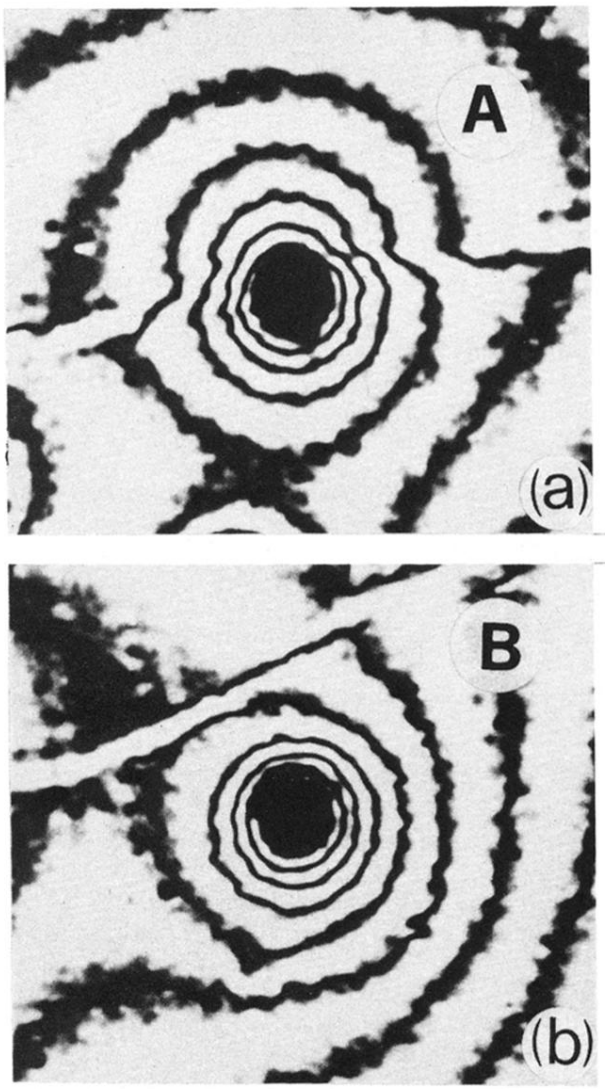

FIG. 6. Four-time phase difference amplification in contour map of the single charged spheres labeled *A* and *B* in Fig. 3.

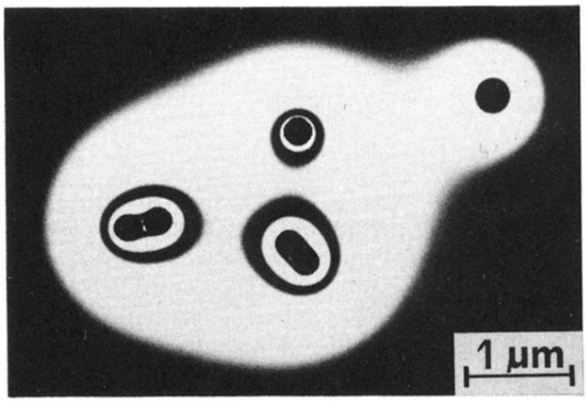

FIG. 7. Simulated contour map for the same distribution of charged spheres as shown in Fig. 3.

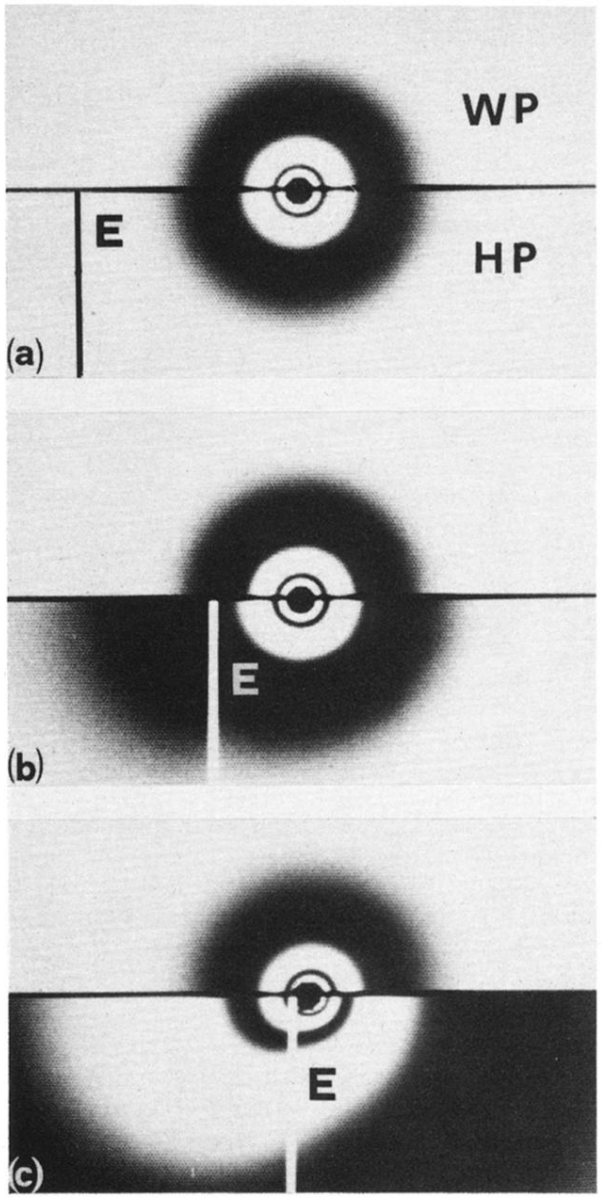

FIG. 9. Comparison of simulated contour maps of a single charged sphere located on the whole conducting plane WP (upper part of each picture) and near the edge (lower part) of a half conducting plane HF. The vertical white line E marks the edge position. Distance between the sphere and the edge: (a) 5 μm; (b) 2 μm; (c) 0.155 μm.